Crustal Accretion and Reworking within the Khanka Massif: Evidence from Hf Isotopes of Zircons in Phanerozoic Granitoids

Xiaoming Zhang[1], Wenliang Xu*[1, 2], Chenyang Sun[1], Ting Xu[1], Feng Wang[1]

1. *College of Earth Sciences, Jilin University, Changchun 130061, China*

2. *State Key Laboratory of Geological Processes and Mineral Resources, China University of Geosciences, Wuhan 430074, China*

DOI: 10.1007/s12583-017-0950-2

Corresponding author: xuwl@jlu.edu.cn **(W.L. Xu)**

E-mail addresses: 770389411@qq.com (**X.M. Zhang**); xuwl@jlu.edu.cn (**W.L. Xu**); suncy0125@foxmail.com (**C.Y. SUN**); 515590170@qq.com (**T. Xu**); jlu_wangfeng@jlu.edu.cn (**F. Wang**)

Postal address: 2199 Jianshe Street, College of Earth Sciences, Jilin University, Changchun 130061, China

ABSTRACT: This paper presents a synthesis and analysis of geochronological, geochemical, and zircon Hf isotopic data of Phanerozoic granitoids within the Khanka Massif, with the aim of revealing the accretion and reworking processes of continental crust within the massif. Zircon U-Pb dating indicates that Phanerozoic granitic magmatism within the Khanka Massif can be subdivided into eight stages: Late Cambrian, Middle–Late Ordovician, middle Silurian, late Carboniferous, early Permian, middle–late Permian to Early Triassic, Late Triassic–Early Jurassic, and Early Cretaceous. The zircon Hf isotopic compositions reveal that crustal accretionary events took place mainly in the Mesoproterozoic and Neoproterozoic. Through time, the zircon $\varepsilon_{Hf}(t)$ values gradually increase, indicating that the Phanerozoic granitic magmas were derived from the melting of progressively less ancient and more juvenile crust. The zircon $\varepsilon_{Hf}(t)$ values exhibit a gradual decrease with the increases in latitude, which implies that the amounts of ancient crustal components within the lower continental crust of the Khanka Massif increased from south to north. At the same latitude range, the zircon Hf isotopic compositions also display some variations. We conclude, therefore, that significant horizontal and vertical heterogeneities existed in the lower continental crust of the Khanka Massif during the Phanerozoic.

KEY WORDS: Khanka Massif; Phanerozoic; granitoid; zircon Hf isotope; crustal accretion and reworking

0 INTRODUCTION

Earth's continental crust is a unique feature among the planets of the solar system. Its formation and evolution is undoubtedly one of the most important subjects of research and debate in the Earth sciences. There is widespread agreement that appreciable volumes of continental crust were generated in the Archean (Dhuime et al., 2012, 2011; Belousova et al., 2010; Hawkesworth and Kemp, 2006; Jahn et al., 2000c; DePaolo et al., 1991; Jacobsen, 1988; Taylor and McLennan, 1985). However, the continents contain two types of tectonic unit, cratons and orogenic belts, and most previous studies on crustal growth have been focused mainly on the cratons, whereas few were concerned with crustal accretion and the reworking processes of microcontinental massifs within orogenic belts.

The Central Asian Orogenic Belt (CAOB) is one of the largest Phanerozoic accretionary orogens in the world (Windley et al., 2007, 1990; Xiao et al., 2004, 2003; Yakubchuk, 2004, 2002; Jahn et al., 2000a, b, c), and studies of the Phanerozoic granitoids within the CAOB have indicated that crustal accretion in this region occurred mainly in the Phanerozoic (Wu et al., 2011, 1999; Jahn et al., 2004, 2000a,b,c). However, more and more data on zircon Hf isotope compositions reveal that the Phanerozoic crustal accretion took place mainly within the Paleozoic orogenic belts of the CAOB, and not within the microcontinental massifs (Tang et al., 2015; Wang et al., 2015), indicating that the importance of Phanerozoic crustal accretion within the CAOB has been grossly overestimated (Luan et al., 2017; Kröner et al.,

2014).

NE China and its adjacent regions, including the Russian Far East, are made up of a series of microcontinental massifs that are separated by orogenic belts, and this region has traditionally been considered the eastern part of the CAOB, located between the Siberian and North China cratons (Sengör and Natal'in, 1996; Sengör et al., 1993). Many granitoids of various ages were formed during the geological evolution of this area, and these granitoids record large amounts of information on crustal accretion and reworking processes within the CAOB (Wu et al., 2011; Rudnick, 1995; DePaolo et al., 1991). However, the answers to questions about how and when the accretion of continental crust within these microcontinental massifs took place remain unclear. The Khanka Massif, as one of the microcontinental massifs within the eastern CAOB, contains numerous Phanerozoic granitoids, and it presents an optimal study area for unraveling the processes of crustal accretion and reworking within these microcontinental massifs. With this in mind, we present here a case study of the processes of crustal accretion and reworking within the microcontinental massifs of the CAOB that is based on spatial and temporal variations in Hf isotopic compositions of zircons from the Phanerozoic granitoids of the Khanka Massif.

1 GEOLOGICAL BACKGROUND

The Paleozoic evolution of the eastern CAOB was dominated by the closure of the Paleo-Asian Ocean and the amalgamation of microcontinental massifs, including, from southeast to northwest, the Khanka, Jiamusi, Songnen–Zhangguangcai Range,

Xing'an, and Erguna massifs (Fig. 1a; Li et al., 2014; Cao et al., 2013; Wang et al., 2012a, b; Wu et al., 2011, 2007, 2002; Meng et al., 2010; Xu et al., 2009; Li, 2006; Li et al., 1999). In contrast, the Mesozoic tectonic evolution of the eastern CAOB was characterized by overprinting of the circum-Pacific and Mongol–Okhotsk tectonic regimes (Tang et al., 2016, 2015; Dong et al., 2014; Xu W L et al., 2013; Xu M J et al., 2013; Yu et al., 2012; Meng et al., 2011).

The Khanka Massif occurs mainly in the Russian Far East, with only a small segment cropping out in NE China. To the north of the Khanka Massif is the Jiamusi Massif, and to the west of that massif, bounded by the Dunhua–Mishan Fault, is the Songnen–Zhangguangcai Range Massif (Fig. 1a; Zhou et al., 2010; Jia et al., 2004). South of the Khanka Massif is the North China Craton (Fig. 1a), bounded by the Yanji Fault (Zhou et al., 2010; Jia et al., 2004), and east of the Khanka Massif is the Sikhote–Alin Orogenic Belt, bounded by the Arsenyev Fault (Fig. 1b; Wang et al., 2016; Jahn et al., 2015; Shao and Tang, 1995).

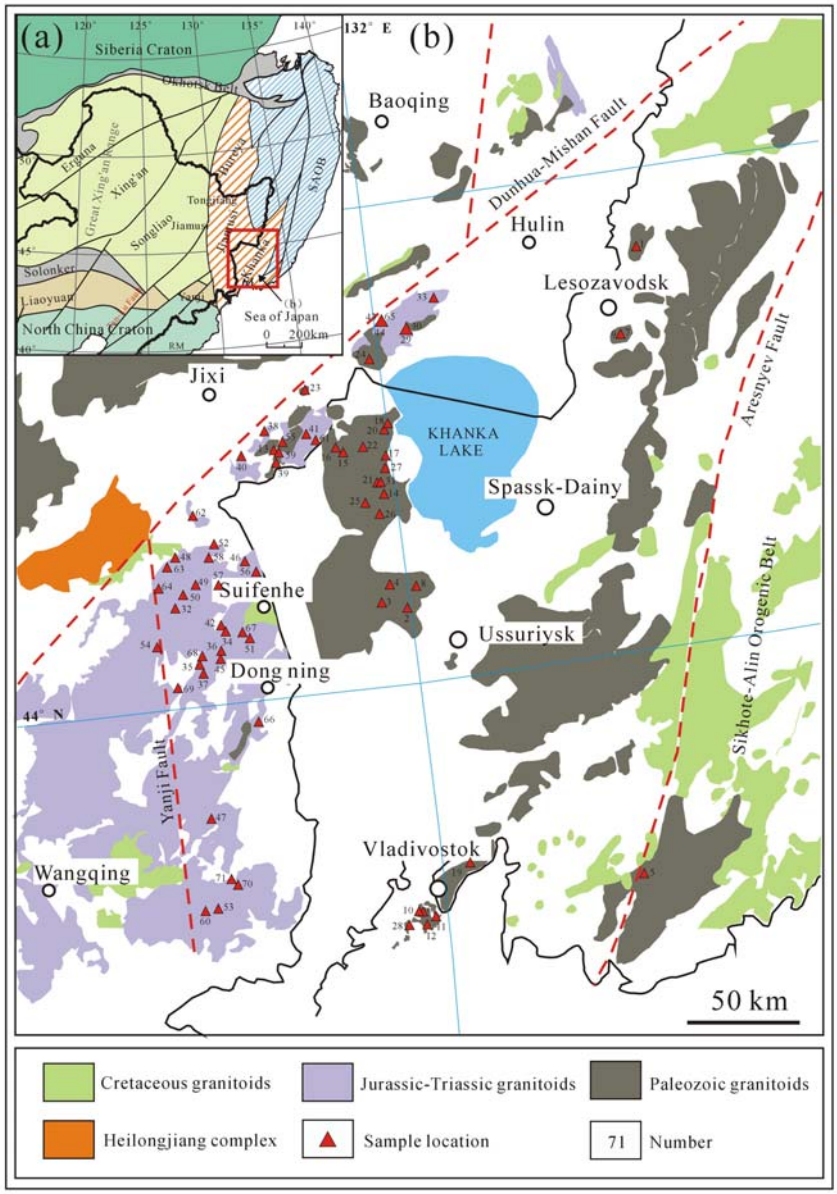

Figure 1. (a) Simplified tectonic divisions of the northeastern Asian continent (Tang et al., 2016; Sun et al., 2013; Wu et al., 2011; Sorokin et al., 2010; Barnes, 2003). (b) Distribution of Phanerozoic granitoids in the study area (modified after Jahn et al., 2015; Xu et al., 2013; Wu et al., 2011; HBGMR, 1993; BGMRJ, 1988).

The Khanka Massif mainly consists of Precambrian microcontinent and some ancient island arcs accreted to the Precambrian microcontinent. The Precambrian terrane only occurs to northeast of the Khanka Massif. In addition, the Precambrian

106 basement includes amphibolite and lower-granulite-facies metamorphic rocks, which
107 is overlain by Paleozoic sedimentary rocks (Tsutsumi et al., 2014; Khanchuk et al.,
108 2010, 2001; Jia et al., 2004; Shcheka et al., 2001; Natal'in, 1993; HBGMR, 1993).
109 The Precambrian basement and Paleozoic cover rocks were intruded by Paleozoic and
110 Mesozoic granitoids, and they were overlain by Mesozoic–Cenozoic sedimentary
111 rocks that are composed mainly of carbonates, clastic sediments, and volcanic rocks
112 (including basalts, andesites, and rhyolites) (Kovalenko, 2006; Khanchuk, 2001;
113 Faure et al., 1995). The intrusive rocks are exposed mainly along the eastern and
114 western margins of the Russian part of the Khanka Massif, and they include small
115 volumes of gneissic gabbro and diorite as well as numerous Paleozoic and Mesozoic
116 granitoid plutons (Kovalenko, 2006).

117 Wang et al. (2016) identified four stages of early Paleozoic magmatic events
118 within the Khanka Massif: Middle Cambrian (~500 Ma), Early Ordovician (~480 Ma),
119 Late Ordovician (~450 Ma), and middle Silurian (~430 Ma). The early Paleozoic
120 magmatic rocks consist of a suite of gneissic granitoids found mainly in the east of
121 Lesozavodsk (Tsutsumi et al., 2014; Khanchuk et al., 2010). The late Paleozoic–early
122 Mesozoic magmatic rocks can be further subdivided into four stages (Wang et al.,
123 2016): (1) early Permian (~285 Ma), as represented by the Chaoxiantun pluton in the
124 Mishan area and the Qianshan pluton in the southern part of the Hunchun area (Yang
125 et al., 2015a; Cao et al., 2011) (2) late Permian (~260 Ma), as represented by a suite of
126 granitoids to the west of Khanka Lake, south of the Vladivostok area (Tsutsumi et al.,
127 2014; Khanchuk et al., 2010), the Wudaogou pluton in the Hunchun area (Cao et al.,

2011), and volcanic rocks, including dacite of the Yanggang Formation in the Jidong area, rhyolite of the Nancun Formation in the Dongning area, and pyroxene andesite of the Tuopangou Formation in the eastern part of Wangqing area; (3) Late Triassic (~202 Ma), as represented along the western margin of the Khanka Massif (Wang et al., 2015; Zhao et al, 2009) by widespread volcanic rocks including pyroxene andesite of the Shuangqiaozi Formation, dacite and rhyolite of the Luoquanzhan Formation, and rhyolite of the Daxinggou Group (Xu et al., 2009); and (4) Early Jurassic (~185 Ma), represented mainly by intermediate–acidic intrusive rocks. The ages of the late Mesozoic magmatic rocks can be subdivided into two stages (Wang et al., 2016): (1) Early Cretaceous (~108 Ma), as represented by a suite of intrusive and volcanic rocks in China (Xu et al., 2013); and (2) Late Cretaceous (~90 Ma), as represented by a suite of andesite and dacite in the Sunfenhe area (Xu et al., 2013; Ji et al., 2007).

2 GEOCHRONOLOGY, DISTRIBUTION, AND GEOCHEMISTRY OF PHANEROZOIC GRANITOIDS IN THE KHANKA MASSIF

2.1 Phanerozoic granitic magmatism events

The Phanerozoic magmatic events are summarized in Supplementary Table 1. According to the U–Pb ages of zircons from granitoids in the Khanka Massif, the Phanerozoic granitic activity can be subdivided into at least eight stages: Late Cambrian, Middle–Late Ordovician, Middle Silurian, late Carboniferous, early Permian, middle–late Permian to Early Triassic, Late Triassic–Early Jurassic, and Early Cretaceous (Fig. 2).

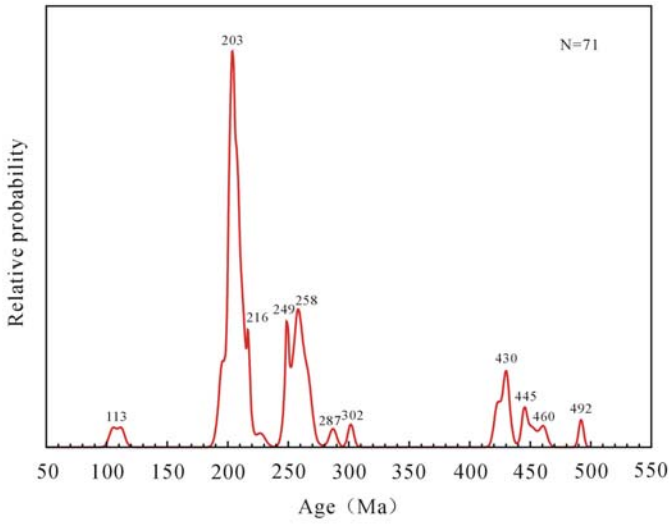

Figure 2**.** Relative probability plot of U–Pb ages of zircons from the Phanerozoic granitoids of the Khanka Massif.

2.2 Distribution and Geochemistry of Phanerozoic granitoids in the Khanka Massif

The Late Cambrian (~492 Ma) granitic rocks are mainly syenogranites that occur ~20 km northeast of Lesozavodsk (Xu et al., 2017). The syenogranites show enrichment in light rare earth elements (LREEs), relative depletion in heavy REEs (HREEs) ($[La/Yb]_N$ = 17.1–23.7), and positive Eu anomalies (Eu/Eu* = 1.97–2.33). They are enriched in large ion lithophile elements (LILEs; e.g., Rb and K) and strongly depleted in high field strength elements (HFSEs; e.g., Nb, Ta, and Ti).

The Middle–Late Ordovician (461–445 Ma) granitic magmatism took place in two periods at ~460 Ma and ~445 Ma (Fig. 2). The ~460 Ma granitic rocks are syenogranites that occur ~40 km north of Ussuriysk (Xu et al., 2017), while the ~445 Ma granitic rocks are granodiorites that occur ~111 km east of Vladivostok (Xu et al., 2017). The ~445 Ma granitic rocks are enriched in LREEs and LILEs (e.g., Rb, Ba and K), and are strongly depleted in HREEs [$(La/Yb)_N$ = 43.2–165] and HFSEs (e.g.,

Nb, Ta, Zr, and Hf), and display pronounced positive Eu and Sr anomalies (Eu/Eu* = 2.22–8.35).

The middle Silurian (431–423 Ma, with a peak at 430 Ma) granitic rocks are monzogranites and granodiorites that occur ~8 km southeast of Lesozavodsk, ~50 km north of Ussuriysk (Xu et al., 2017), and to the south of Vladivostok (Tsutsumi et al., 2014). The ~430 Ma granodiorites and biotite monzogranites exhibit depletion in HREEs ($[La/Yb]_N$ = 29.0–98.1) and HFSEs (e.g., Nb, Ta and Ti), along with negative Eu anomalies (Eu/Eu* = 0.47–0.88).

The late Carboniferous (~302 Ma) granitic rocks are granites (Fig. 2) that occur to the south of Vladivostok (Tsutsumi et al., 2014).

The early Permian (~287 Ma) granitic rocks are monzogranites (Fig. 2) that are found in Chaoxiantun Village (Yang et al., 2015a). The ~287 Ma monzogranites are enriched in LREEs, relative depleted in HREEs($[La/Yb]_N$ = 8.11) and HFSEs (e.g., Nb, Ta and Ti), along with negative Eu anomalies (Eu/Eu* = 0.61).

The middle–late Permian to Early Triassic (268–249 Ma) granitic magmatism took place mainly in two periods at ~258 Ma and ~249 Ma (Fig. 2). The ~258 Ma granitic rocks are granodiorites and granite porphyries that occur at Shuangyehu (Yang et al., 2015a), Yangtianzhai (Yang et al., 2015a), and Ryazanovka (Khankchuk et al., 2010). The ~249 Ma granitic rocks are granodiorites that occur at Vladivostok (Tsutsumi et al., 2014) and Ryazanovka (Khankchuk et al., 2010). The granodiorites show enrichment in LREEs and LILEs (e.g., Rb and K), depletion in HREEs ($[La/Yb]_N$ = 15.53-15.84) and HFSEs (e.g., Nb, Ta), and minor negative Eu anomalies

(Eu/Eu* = 0.94–1.00). The granite porphyries exhibit enrichment in LREEs, relative depletion in HREEs ($[La/Yb]_N$ = 7.01).

The Late Triassic–Early Jurassic (228–195 Ma) granitic magmatism took place mainly in two periods at ~216 Ma and ~203 Ma (Fig. 2). The ~216 Ma granitic rocks are syenogranites, monzogranites, and associated rhyolites that occur in Shanhezi (Wu et al., 2011), on Daxu Mountain (Wu et al., 2011), and in Wupai Village (Yang et al., 2015).The ~203 Ma granitic rocks are syenogranites, monzogranites, and granodiorites that occur in the Suifenhe area, along with associated rhyolites. The Late Triassic–Early Jurassic granitoids are enriched in LREEs and LILEs (e.g., Rb and K), depleted in HREEs ($[La/Yb]_N$ = 4.49-6.77) and HFSEs (e.g., Nb, Ta, and Ti), and have variable negative Eu anomalies (Eu/Eu* = 0.08-0.92).

The Early Cretaceous (113 Ma) granitic rocks are granodiorites (Fig. 2) that occur in the Xiaoxinancha area of Hunchun City (Sun et al., 2008).

In summary, the Phanerozoic granitoids in the Khanka Massif mainly consist of a suite of granodiorites, monzogranites, and syenogranites. On the TAS diagram, they fall in the fields of granodiorite and granite, and chemically belong to the subalkaline series (Fig. 3). They have high SiO_2 (>65 wt%) and Al_2O_3 contents (12.47-17.11), low $Mg^{\#}$ (4-45), Co (0.31-7.18 ppm) and Ni (0.46-7.64 ppm) contents. These geochemical characteristics suggest that the Phanerozoic granitoids in the Khanka Massif could be derived from partial melting of deep crustal material (Lu and Xu, 2011).

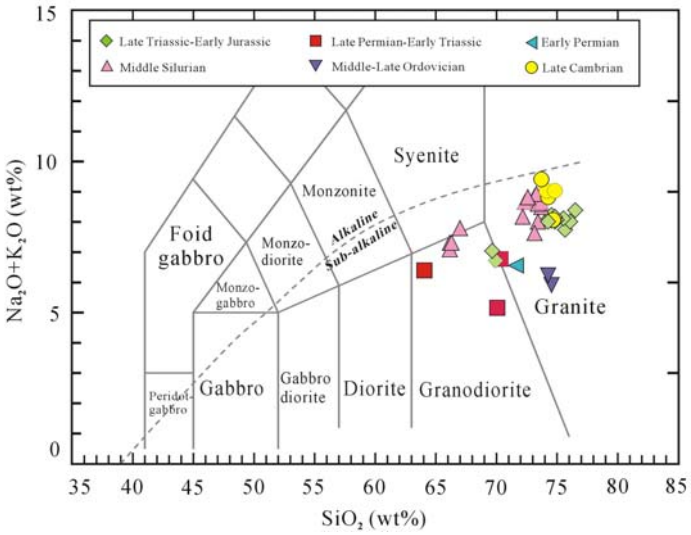

Figure 3. Plots of SiO_2 (wt%) versus (Na_2O + K_2O) (wt%) for the Phanerozoic granitoids of the Khanka Massif (the field boundaries in the diagram are from Le Maitre, 1989).

3 HF ISOTOPIC COMPOSITIONS OF ZIRCONS IN PHANEROZOIC GRANITOIDS OF THE KHANKA MASSIF

For this paper we compiled the recently published Hf isotopic data of zircons in Phanerozoic granitoids of the Khanka Massif. We do not consider the data of

218 inherited zircons, and we discuss only the Hf isotopic data of zircons with ages that
219 represent the timing of crystallization of the granitoids. The Hf isotope data are listed
220 in Supplementary Table 2. In the Table 2, depleted mantle model ages (T_{DM}) were
221 calculated using the measured $^{176}Lu/^{177}Hf$ ratios, referred to a model depleted mantle
222 with a present-day $^{176}Hf/^{177}Hf$=0.28325, similar to that of average MORB (*Nowell et*
223 *al., 1998*) and $^{176}Lu/^{177}Hf$=0.0384 (*Griffin et al., 2000*). *Griffin et al. (2002)* presented
224 a more realistic estimate (T_{DM2}) of the age of the source rocks for the magmas,
225 derived by projecting the initial $^{176}Hf/^{177}Hf$ of the zircon back to the depleted mantle
226 model growth curve, assuming a mean crustal value for $^{176}Lu/^{177}Hf$=0.015. This
227 average crustal value was used as the standard to analyze the zircon Lu–Hf results
228 presented in this paper.

229 Nearly all the Hf isotopic data of zircons in the Phanerozoic granitoids fall in the
230 field of the CAOB (Fig. 4a), regardless of the specific area the granitoid comes from.
231 The Hf isotopic compositions are similar to those of zircons from other Phanerozoic
232 igneous rocks in the CAOB, but they differ from zircons of Neoarchean and
233 Paleoproterozoic age that are found in Paleozoic–Mesozoic units of the Yanshan
234 Fold-and-Thrust Belt (YFTB) of the NCC (Yang et al., 2006; Xiao et al., 2004).

235 **3.1 Hf isotopic compositions of zircons from the Late Cambrian granitoids**

236 The $^{176}Hf/^{177}Hf$ ratios of 15 zircon grains from the Late Cambrian (~492 Ma)
237 granitoids vary from 0.282411 to 0.282488, corresponding to $\varepsilon_{Hf}(t)$ values and
238 two-stage model (T_{DM2}) ages of –2.2 to 0.5 (Fig. 4b) and 1430 to 1600 Ma (Fig. 4c),
239 respectively (Xu et al., 2017). The average two-stage model (T_{DM2}) age is 1522 Ma.

240 **3.2 Hf isotopic compositions of zircons from the Middle–Late Ordovician**
241 **granitoids**

242 The $^{176}Hf/^{177}Hf$ ratios of 22 zircon grains from the Middle–Late Ordovician
243 (~461 Ma and ~445 Ma) granitoids vary from 0.282556 to 0.282693. Their $\varepsilon_{Hf}(t)$
244 values and T_{DM2} ages range from 1.8 to 6.6 (Fig.4b) and from 1020 to 1311 Ma (Fig.
245 4c), respectively (Xu et al., 2017). The average T_{DM2} age is 1222 Ma.

246 **3.3 Hf isotopic compositions of zircons from the middle Silurian granitoids**

247 The $^{176}Hf/^{177}Hf$ ratios of 29 zircon grains from the middle Silurian (~430 Ma)
248 granitoids vary from 0.282357 to 0.282711. Their $\varepsilon_{Hf}(t)$ values and T_{DM2} ages range
249 from –5.4 to 5.8 (Fig. 4b) and from 1045 to 1757 Ma (Fig. 4c), respectively (Xu et al.,
250 2017). The average T_{DM2} age is 1451 Ma.

251 **3.4 Hf isotopic compositions of zircons from the early Permian granitoids**

252 The $^{176}Hf/^{177}Hf$ ratios of 13 zircon grains from the early Permian granitoids vary
253 from 0.282582 to 0.282652. Their $\varepsilon_{Hf}(t)$ values and T_{DM2} ages range from –0.6 to 1.8
254 (Fig. 4b) and from 1189 to 1342 Ma (Fig. 4c), respectively (Yang et al., 2015a). The
255 average T_{DM2} age is 1252 Ma.

256 **3.5 Hf isotopic compositions of zircons from the late Permian–Early Triassic**
257 **granitoids**

258 The $^{176}Hf/^{177}Hf$ ratios for 35 zircon grains from the late Permian–Early Triassic
259 (~258 Ma and ~249 Ma) granitoids vary from 0.282601 to 0.282723. Their $\varepsilon_{Hf}(t)$
260 values and T_{DM2} ages range from –0.6 to 3.7 (Fig. 4b) and from 1048 to 1318 Ma (Fig.
261 4c), respectively (Liu et al., 2017; Yang et al., 2015a). The average T_{DM2} age is 1197

Ma.

3.6 Hf isotopic compositions of zircons from the Late Triassic–Early Jurassic granitoids

The $^{176}Hf/^{177}Hf$ ratios of 130 zircons from the Late Triassic–Early Jurassic (~218 to ~199 Ma) granitoids vary from 0.282669 to 0.282913. Their $\varepsilon_{Hf}(t)$ values and T_{DM2} ages range from 0.8 to 9.3 (Fig. 4b) and from 720 to 1197 Ma (Fig. 4c), respectively (Liu et al., 2017; Jing et al., 2015; Wang et al., 2015; Yang et al., 2015a; Yang et al., 2015b). The average T_{DM2} age is 908 Ma.

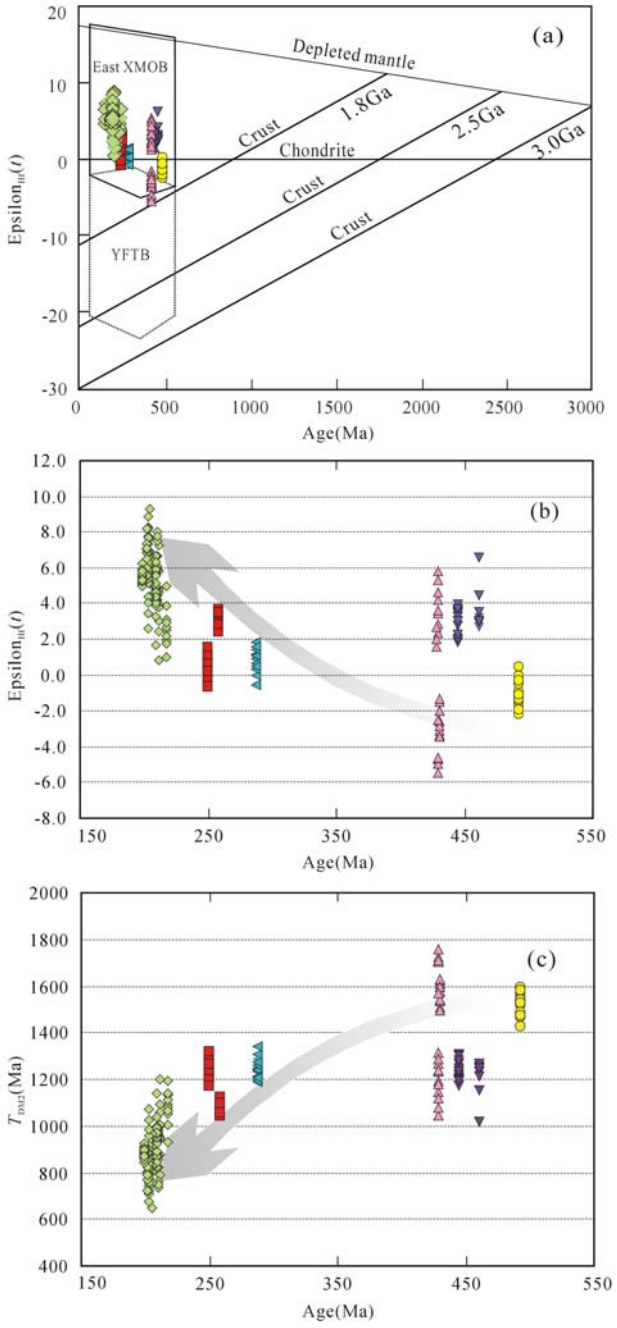

270

271 Figure 4**.** (a) Correlations between $\varepsilon_{Hf}(t)$ values and the ages of zircons from the

272 Phanerozoic granitoids in the Khanka Massif (CAOB = Central Asian Orogenic Belt;

273 YFTB = Yanshan Fold-and-Thrust Belt) (Yang et al., 2006). (b) Detailed diagram of

274 the ages of zircons versus values of $\varepsilon_{Hf}(t)$ (legend as for Fig. 3). (c) Detailed diagram

275 of the ages of zircons versus values of T_{DM2} (Ma) (legend as for Fig. 3).

4 SPATIAL–TEMPORAL VARIATIONS IN ZIRCON HF ISOTOPIC COMPOSITIONS AND THE ACCRETION AND REWORKING OF CONTINENTAL CRUST

4.1 Temporal variations in Hf isotopic compositions of zircons from the Phanerozoic granitoids

The Hf isotopic compositions of zircons from the Phanerozoic granitoids show obvious trends that correlate with time. As the ages of the Phanerozoic granitoids decrease (Late Cambrian to Middle–Late Ordovician to middle Silurian to early Permian to middle–late Permian–Early Triassic to Late Triassic–Early Jurassic), the $\varepsilon_{Hf}(t)$ values of their zircons gradually increase (Fig. 4b), whereas the T_{DM2} ages gradually decrease (Mesoproterozoic to Neoproterozoic) (Fig. 4c). These trends suggest that the sources of the granitic magmas that were intruded into the Khanka Massif changed gradually to an increasingly juvenile crust throughout the Paleozoic and early Mesozoic.

4.2 Spatial variations in Hf isotopic compositions of zircons from the Phanerozoic granitoids

The $\varepsilon_{Hf}(t)$ values of zircons from the Phanerozoic granitoids tend to decrease with increasing latitude (Fig. 5a), which implies that the components of ancient continental crust in the source area increased gradually from south to north (Fig. 5b). However, within the same range of latitude, the $\varepsilon_{Hf}(t)$ values of zircons from the Phanerozoic granitoids also exhibit some variations (Fig. 5a). For example, the

Phanerozoic granitoids located at a latitude of 45.5° in the western part of the Khanka Massif have higher zircon $\varepsilon_{Hf}(t)$ values than those in the eastern part of the Khanka Massif. Moreover, as the ages of the Phanerozoic granitoids at the latitude of 45.5° decrease, the $\varepsilon_{Hf}(t)$ values of their zircons gradually increase (gray shading in Fig. 5a), whereas their T_{DM2} ages gradually decrease (gray shading in Fig. 5b).

In addition, the $\varepsilon_{Hf}(t)$ values of zircons from the Phanerozoic granitoids tend to decrease with increasing longitude (Fig. 5c), which implies that the components of ancient continental crust in the source area gradually increased from west to east (Fig. 5d).

Taking into account all these observations, we conclude that the lower continental crust within the Khanka Massif exhibits heterogeneities in chemical composition in both the horizontal and vertical directions.

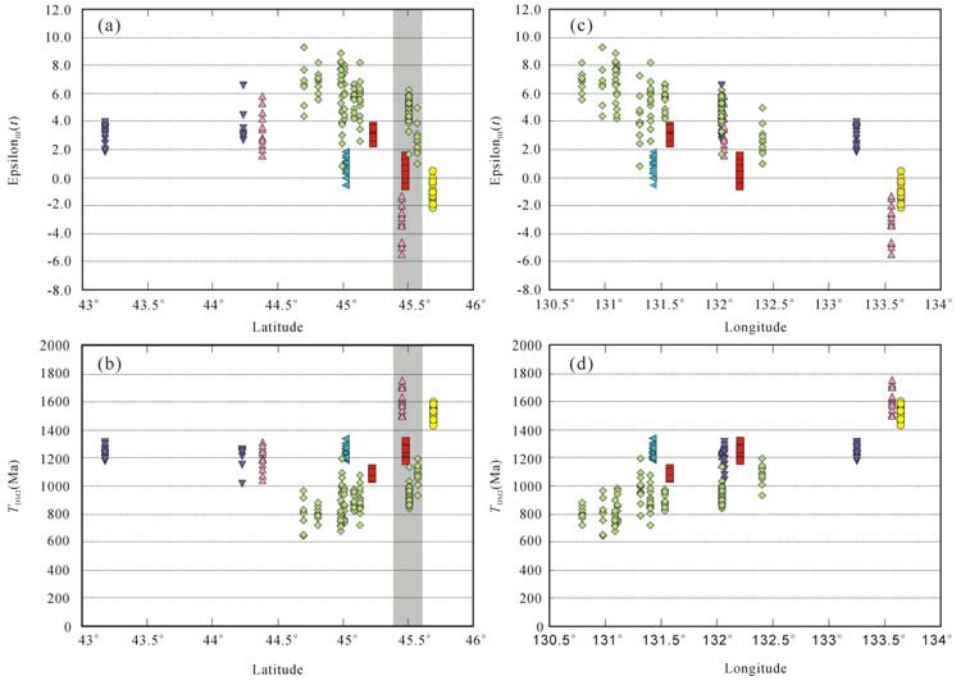

Figure 5. Plots of the latitudes and Longitudes of sampling locations versus $\varepsilon_{Hf}(t)$ values and T_{DM2} ages.

4.3 Accretion and reworking of continental crust within the Khanka Massif

The CAOB is the largest Phanerozoic accretionary orogenic belt in the world, and this observation is consistent with the Nd isotopic and zircon Hf isotopic compositions of the Phanerozoic granitoids (Wu et al., 2011, 2003, 1999; Jahn et al., 2004, 2000a, b, c; Xiao et al., 2003). However, more and more research now indicates that the Phanerozoic crustal accretion probably took place in Paleozoic orogenic belts between the microcontinental massifs of the CAOB, rather than within the microcontinental massifs themselves, particularly in the eastern CAOB (Sun et al., 2017; Wang et al., 2017, 2016). In previous studies, the amount of continental crust accreted in the CAOB during the Phanerozoic has been overestimated (Kröner et al., 2014). The question then arises: when did crustal accretion within the microcontinental massifs take place? The Khanka Massif, as one of the microcontinental massifs of the eastern CAOB, is an ideal site for studying the crustal accretion within the microcontinental massifs of this orogenic belt, because numerous Phanerozoic granitoids occur within the massif (Xu et al., 2017).

The reconstruction of crustal growth curve is based mainly on the detrital zircon Hf isotope (Dhuime et al., 2012; Condie et al., 2011; Condie and Aster, 2010), especial those from rivers could reflect the crustal growth of the blocks that the rivers occur (Liu et al., 2017; Wang et al., 2011, 2009; Belousova et al., 2010). However, the detrital mineral suffered from physical-chemical weathering, and transportation of river or wind. Finally, they deposited in the sedimentary area, were buried and formed rock. There are many uncertain factors in the long and complicated geological history,

335 which produce some deviation about the age of detrital zircon (Guo et al., 2017).
336 Additionally, the some crustal growth curves are smooth in part because these models
337 are typically based on radiogenic isotope ratios (whole-rock Sr-Nd-Pb isotopes) of
338 sediments and sedimentary rocks (Mclennan, 2001; Davies et al., 1985; Allègre and
339 Rousseau, 1984; O'Nions et al., 1983; Armstrong, 1981). Such samples reflect the
340 history of the crust over long periods of time, but they may also result in hybrid crust
341 generation ages that are the result of mixing processes rather than real magmatic
342 events. Igneous rocks preserve the ages of the specific events in which new
343 continental crust may have been generated, although this record may not be complete
344 (Hawkesworth and Kemp, 2006). Taken together, we consider that because these
345 granitoids are chiefly derived from partial melting of the lower crust, the Hf isotopic
346 compositions of magmatic zircons from these granitoids basically record the growth
347 and reworking history of the lower continental crust within the Khanka Massif.

348 The two-stage model (T_{DM2}) ages of zircons in the Phanerozoic granitoids of the
349 Khanka Massif indicate that crustal accretion took place mainly during three stages: 1)
350 Mesoproterozoic, 2) Neoproterozoic, and 3) to a lesser extent, late Paleoproterozoic
351 (Fig. 6).

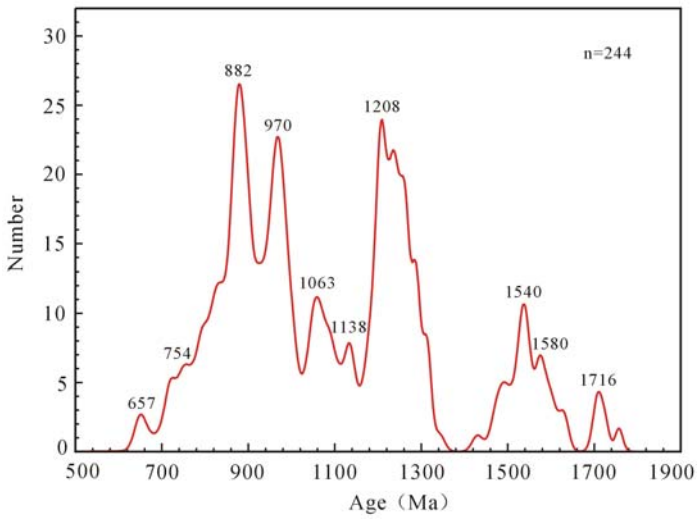

352

353 Figure 6**.** Relative probability plot of two-stage model (T_{DM2}) ages of zircons from the

354 Phanerozoic granitoids in the Khanka Massif.

355 We calculate the cumulative growth curve of continental crust for the Khanka

356 Massif by the Hf isotopic compositions of zircons from the Phanerozoic granitoids

357 (Fig. 7). The curve indicates that the accretion of continental crust within the Khanka

358 Massif took place during the Proterozoic, which differs from the traditional viewpoint

359 that the accretion of continental crust within the CAOB took place mainly in the

360 Phanerozoic (Jahn et al., 2004, 2000; Wu et al., 2011, 1999) as well as continental

361 growth models within cratonic regions (Cawood et al., 2013; Wang et al.,2011, 2009)

362 (Fig. 7). These results also indicate that the Khanka Massif has a Precambrian

363 basement, and more obviously so during the early Paleozoic.

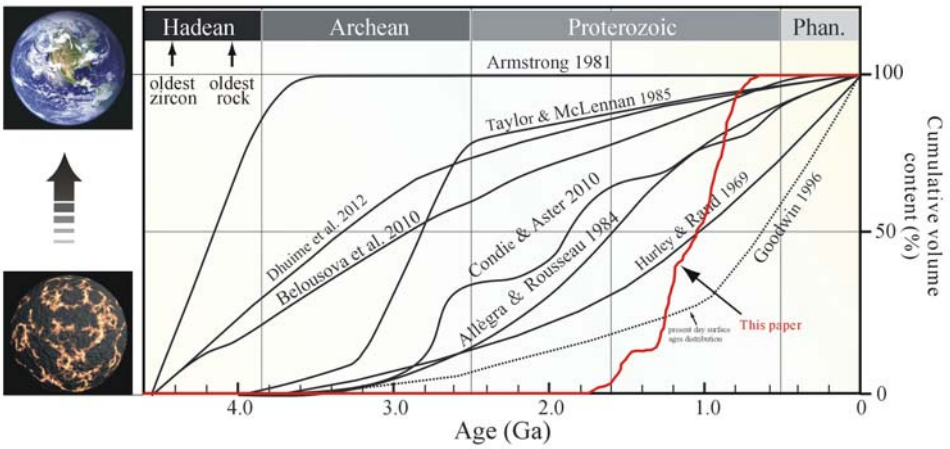

364

365 Figure 7**.** Crustal growth curve of the Khanka Massif (modified after Cawood et al.,

366 2013)

367 The Hf isotopic compositions of zircons from the Phanerozoic granitoids not

368 only reveal the nature of accretionary process in the lower continental crust of the

369 microcontinental massifs, but also reflect the processes of reworking of the lower

370 continental crust. The formation of granitoids results mainly from the reworking of

371 the lower continental crust (Sun et al., 2017). How, then, did these Phanerozoic

372 granitoids form, and how was the lower crust reworked during the formation of these

373 granitoids?

374 The zircon two-stage model (T_{DM2}) ages (Fig. 4c), together with the changes in

375 $\varepsilon_{Hf}(t)$ values with latitude (Fig. 5), suggest that the Late Cambrian and middle Silurian

376 granitoids in the northeastern part of the Khanka Massif originated mainly from the

377 reworking of a late Paleoproterozoic–early Mesoproterozoic (1430–1757 Ma) lower

378 crust, whereas the Middle–Late Ordovician and middle Silurian granitoids in the

379 southern part of the Khanka Massif resulted from the reworking of a Mesoproterozoic

380 (1020–1313 Ma) lower crust. The early Permian–Early Triassic granitoids along the

western margin of the Khanka Massif were derived chiefly from the reworking of late Mesoproterozoic lower crust, whereas the Late Triassic–Early Jurassic granitoids were derived mainly from the reworking of a Neoproterozoic lower crust (Fig. 4c; Supplementary Table 2). We conclude, therefore, that the Phanerozoic granitoids of the Khanka Massif were generated by the reworking of lower continental crustal material with different ages, and that the crustal material that was reworked decreased in age progressively throughout the Phanerozoic.

5 CONCLUSIONS

(1) The periods of Phanerozoic granitic magmatism in the Khanka Massif can be subdivided into at least eight stages: Late Cambrian, Middle–Late Ordovician, middle Silurian, late Carboniferous, early Permian, middle–late Permian to Early Triassic, Late Triassic–Early Jurassic, and Early Cretaceous.

(2) The Hf isotopic compositions of zircons from the Phanerozoic granitoids reveal that the accretion of the lower continental crust in the Khanka Massif took place mainly in the Mesoproterozoic and Neoproterozoic, and to a lesser extent in the Paleoproterozoic.

(3) The Khanka Massif is an ancient microcontinent with a Precambrian basement.

(4) The repeated reworking of the lower crust of the Khanka Massif resulted in the source of the Phanerozoic granitoids becoming progressively less ancient and more juvenile over time.

ACKNOWLEDGMENTS

We thank the staff of the State Key Laboratory of Geological Processes and Mineral Resources, China University of Geosciences, Wuhan, for their advice and assistance during U–Pb zircon dating and the staff of the Institute of Geology and Geophysics, Chinese Academy of Sciences, Beijing, China for help in the Hf isotope analyses. This work was financially supported by the National Natural Science Foundation of China (Grants 41772047 and 41330206), the Graduate Innovation Fund of Jilin University (2017034), and the Opening Foundation of the State Key Laboratory of Geological Processes and Mineral Resources, China University of Geosciences (Wuhan) (GPMR201503).

REFERENCES CITED

Allègre, C. J., Rousseau, D., 1984. The Growth of Continent through Geological Time Studied by Nd Isotope Analysis of Shales. *Earth and Planetary Science Letters*, 67(1): 19–34

Armstrong, R. A., 1981. Radiogenic Isotopes: The Case for Crustal Recycling on a Near-Steady-State No-Continental-Growth Earth. *Philosophical Transactions of the Royal Society of London, Series A, Mathematical and Physical Sciences*, 301(1461): 443–472

Barnes, G. L., 2003. Origins of the Japanese Islands: The New “Big Picture”. *Japan Review*, 15: 3–50

Belousova, E. A., Kostitsyn, Y. A., Griffin, W. L., et al., 2010. The Growth of the Continental Crust: Constraints from Zircon Hf Isotope Data. *Lithos*, 119(3): 457–466

Boynton, W. V., 1984. Geochemistry of the Rare Earth Elements: Meteorite Studies. In: Henderson, P., ed., Rare Earth Element Geochemistry. Elsevier, Amsterdam. 63–114

BGMRJ (Bureau of Geology and Mineral Resources of Jilin Province)., 1997. Stratigraphy of Jilin Province. China University of Geosciences Press, Wuhan. 10–13 (in Chinese)

Cao, H. H., Xu, W. L., Pei, F. P., et al., 2011. Permian Tectonic Evolution in Southwestern Khanka Massif: Evidence from Zircon U–Pb Chronology, Hf Isotope and Geochemistry of Gabbro and Diorite. *Acta Geologica Sinica* (English edition), 85(6): 1390–1402

Cao, H. H., Xu, W. L., Pei, F. P., et al., 2013. Zircon U-Pb Geochronology and Petrogenesis of the Late Paleozoic-Early Mesozoic Intrusive Rocks in the Eastern Segment of the Northern Margin of the North China Block. *Lithos*, 170–171(6): 191–207

Cawood, P. A., Wang, Y., Xu, Y., et al., 2013. Locating South China in Rodinia and Gondwana: A Fragment of Greater India Lithosphere? *Geology*, 41(8): 903–906

Condie, K. C., Aster, R. C., 2010. Episodic Zircon Age Spectra of Orogenic Granitoids: The Supercontinent Connection and Continental Growth. *Precambrian Research*, 180(3): 227–236

447 Condie, K. C., Bickford, M. E., Aster, R. C., et al., 2011. Episodic Zircon Ages, Hf
448 Isotopic Composition, and the Preservation Rate of Continental Crust.
449 *Geological Society of America Bulletin*, 123(5–6): 951–957
450 Davies, G., Gledhill, A., Hawkesworth, C., 1985. Upper Crustal Recycling in
451 Southern Britain: Evidence from Nd and Sr Isotopes. *Earth and Planetary*
452 *Science Letters*. 75(1): 1–12
453 Depaolo, D. J., Linn, A. M., Schubert, G., 1991. The Continental Crustal Age
454 Distribution: Methods of Determining Mantle Separation Ages from Sm-Nd
455 Isotopic Data and Application to the Southwestern United States. *Journal of*
456 *Geophysical Research*, 96: 2071–2088
457 Dhuime, B., Hawkesworth, C. J., Cawood, P. A., et al., 2012. A Change in the
458 Geodynamics of Continental Growth 3 Billion Years Ago. *Science*, 335(6047):
459 1334-1336
460 Dhuime, B., Hawkesworth, C. J., Cawood, P. A., 2011. When Continents Formed.
461 *Science*, 331(6014): 154–155
462 Dong, Y., Ge, W. C., Yang, H., et al., 2014. Geochronology and Geochemistry of
463 Early Cretaceous Volcanic Rocks from the Baiyingaolao Formation in the
464 Central Great Xing'an Range, NE China, and Its Tectonic Implications. *Lithos*,
465 205: 168–184
466 Faure, M., Natal'in, B. A., Monie, P., et al., 1995. Tectonic Evolution of the Anuy
467 Metamorphic Rocks (SikhoteAlin, Russia) and Their Place in the Mesozoic
468 Geodynamic Framework of East Asia. *Tectonophysics*, 241(3): 279–301

469 Goodwin, A. M., 1996. Principles of Precambrian Geology. Academic Press, London.
470 281–318
471 Griffin, W. L., Pearson, N. J., Belousova, E., et al., 2000. The Hf Isotope Composition
472 of Cratonic Mantle: LAM–MC–ICPMS Analysis of Zircon Megacrysts in
473 Kimberlites. *Geochimica Et Cosmochimica Acta*, 64(1): 133–147
474 Griffin, W. L., Wang, X., Jackson, S. E., et al., 2002. Zircon Chemistry and Magma
475 Mixing, SE China: In-situ Analysis of Hf Isotopes, Tonglu and Pingtan Igneous
476 Complexes. *Lithos*, 61: 237–269
477 Guo, P., Liu, C. Y., Wang, J. Q., et al., 2017. Considerations on the Application of
478 Detrital-Zircon Geochronology to Sedimentary Provenance Analysis. *Acta*
479 *Sedimentologica Sinica*, 35(1): 46-55 (in Chinese with English Abstract)
480 Hawkesworth, C. J., Kemp, A. I. S., 2006. The Differentiation and Rates of
481 Generation of the Continental Crust. *Chemical Geology*, 226(3): 134–143
482 HBGMR (Heilongjiang Bureau of Geology Mineral Resources)., 1993. Regional
483 Geology of Heilongjiang Province. Geological Publishing House, Beijing. 1–734
484 (in Chinese with English Abstract)
485 Hurley, P. M., Rand, J. M., 1969. Pre-drift Continental Nuclei. *Science*, 164(3885):
486 1229–1242
487 Jacobsen, S. B., 1988. Isotopic and Chemical Constraints on Mantle-crust Evolution.
488 *Geochimica Et Cosmochimica Acta*, 52(6): 1341–1350
489 Jahn, B. M., Capdevila, R., Liu, D. Y., et al., 2004. Sources of Phanerozoic Granitoids
490 in the Transect Bayanhongor-Ulaan Baatar, Mongolia: Geochemical and Nd

Isotopic Evidence, and Implications for Phanerozoic Crustal Growth. *Journal of Asian Earth Sciences*, 23(5): 629–653

Jahn, B. M., Wu, F. Y., Chen, B., 2000a. Massive Granitoid Generation in Central Asia: Nd Isotopic Evidence and Implication for Continental Growth in the Phanerozoic. *Episodes*, 23(2): 82–92

Jahn, B. M., Wu, F. Y., Chen, B., 2000c. Granitoids of the Central Asian Orogenic Belt and Continental Growth in the Phanerozoic. *Transactions of the Royal Society of Edinburgh: Earth Sciences*, 91(1–2): 181–193

Jahn, B. M., Wu, F. Y., Hong, D., 2000b. Important Crustal Growth in the Phanerozoic: Isotopic Evidence of Granitoids from East-central Asia. *Journal of Earth System Science*, 109(1): 5–20

Jahn, B. M., Valui, G., Kruk, N., et al., 2015. Emplacement Ages, Geochemical and Sr–Nd–Hf Isotopic Characterization of Mesozoic to Early Cenozoic Granitoids of the Sikhote-Alin Orogenic Belt, Russian Far East: Crustal Growth and Regional Tectonic Evolution. *Journal of Asian Earth Sciences*, 111: 872–918

Ji, W. Q., Xu, W. L., Yang, D. B., et al., 2007. Chronology and Geochemistry of Volcanic Rocks in the Cretaceous Suifenhe Formation in Eastern Heilongjiang, China. *Acta Geologica Sinica* (English edition), 81(2): 266–277

Jia, D. C., Hu, R. Z., Lu, Y., et al., 2004. Collision Belt between the Khanka Block and the North China Block in the Yanbian Region, Northeast China. *Journal of Asian Earth Sciences*, 23(2): 211–219

Jing, H. X., Sun, D. Y., Gou, J., et al., 2015. Chronology, Geochemistry and Hf

513 Isotope of Granite from Southern Xingkai Block. *Journal of China University*
514 *Geosciences*, 40(6): 982–994 (in Chinese with English Abstract)
515 Khanchuk, A. I., Sakhno, V. G., Alenicheva, A. A., 2010. First SHRIMP U–Pb
516 Zircon Dating of Magmatic Complexes in the Southwestern Primor'e Region.
517 *Doklady Earth Sciences*, 431(2): 424–428
518 Khanchuk, A. I., 2001. Pre-Neogene Tectonics of the Sea of Japan region: A View
519 from the Russian Side. *Earth Science* (*Chikyu Kagaku*), 55(5): 275–291
520 Kovalenko, S. V., 2006. State Geological Map of Russian Federation, Scale 1:1 000
521 000 (3rd Generation). Far East Ser. Sheet L-52 (Boundary), L-53 (Khanka),
522 K-53 (Nakhodka) (in Russian)
523 Kröner, A., Kovach, V., Belousova, E., et al., 2014. Reassessment of Continental
524 Growth during the Accretionary History of the Central Asian Orogenic Belt.
525 *Gondwana Research*, 25(1): 103–125
526 Li, J. Y., Niu, B. G., Song, B., et al., 1999. Crustal Formation and Evolution of
527 Nothern Changbai Mountains. Geological Publishing House, Beijing. 1–137 (in
528 Chinese with English Abstract)
529 Li, J. Y., 2006. Permian Geodynamic Setting of Northeast China and Adjacent
530 Regions: Closure of the Paleo-Asian Ocean and Subduction of the Paleo-Pacific
531 Plate. *Journal of Asian Earth Sciences*, 26(3): 207–224
532 Li, Y., Xu, W. L., Wang, F., et al., 2014. Geochronology and Geochemistry of Late
533 Paleozoic Volcanic Rocks on the Western Margin of the Songnen-Zhangguangcai
534 Range Massif, NE China: Implications for the Amalgamation History of the

Xing'an and Songnen-Zhangguangcai Range Massifs. *Lithos*, 205: 394–410

Liu, K., Zhang, J. J., Wilde, S. A., et al., 2017. Initial Subduction of the Paleo-Pacific Oceanic Plate in NE China: Constraints from Whole-rock Geochemistry and Zircon U–Pb and Lu–Hf Isotopes of the Khanka Lake Granitoids. *Lithos*, 274–275: 254–270

Lu, L. Z., Xu, W. L., 2011. Petrography. Geological Publishing House, Beijing. 377 (in Chinese)

Luan, J. P., Xu, W. L., Wang, F., et al., 2017. Age and Geochemistry of Neoproterozoic Granitoids in the Songnen-Zhangguangcai Range Massif, NE China: Petrogenesis and Tectonic Implications. *Journal of Asian Earth Sciences*, 148: 265–276

Maitre, R. W. L., 1989. A Classification of Igneous Rocks and Glossary of Terms: Recommendations of the International Union of Geological Sciences Subcommission on the Systematics of Igneous Rocks. Blackwell Scientific Publications, Oxford. 193

McLennan, S. M., 2001. Relationships between the Trace Element Composition of Sedimentary Rocks and Upper Continental Crust. *Geochemistry Geophysics Geosystems*, 2(4): 203–236

Meng, E., Xu, W. L., Pei, F. P., et al., 2010. Detrital-zircon Geochronology of Late Paleozoic Sedimentary Rocks in Eastern Heilongjiang Province, NE China: Implications for the Tectonic Evolution of the Eastern Segment of the Central Asian Orogenic Belt. *Tectonophysics*, 485: 42–51

557 Meng, E., Xu, W. L., Yang, D. B., et al., 2011. Zircon U-Pb Chronology,
558 Geochemistry of Mesozoic Volcanic Rocks from the Lingquan Basin in
559 Manzhouli Area, and its Tectonic Implications. *Acta Petrologica Sinica*, 27(4):
560 1209–1226 (in Chinese with English Abstract)
561 Natal'in, B. A., 1993. History and Modes of Mesozoic Accretion in Southeastern
562 Russia. *Island Arc*, 2(1): 15–34
563 Nowell, G. M., Kempton, P. D., Noble, S. R., et al., 1998. High Precision Hf Isotope
564 Measurements of MORB and OIB by Thermal Ionization Mass Spectrometry:
565 Insights into the Depleted Mantle. *Chemical Geology*, 149: 211-233
566 O'Nions, R. K., Hamilton, P. J., Hooker, P. J., 1983. A Nd Isotope Investigation of
567 Sediment Related to Crustal Development in the British Isles. *Earth and*
568 *Planetary Science Letters*, 63(2): 229-240
569 Rudnick, R. L., 1995. Making Continental Crust. *Nature*, 378: 571–578
570 Sengör, A. M. C., Natal'in, B. A., 1996. Paleotectonics of Asia: Fragments of a
571 Synthesis. Cambridge University Press, Cambridge. 486–640
572 Sengör, A. M. C., Natal'in, B. A., Burtman, V. S., 1993. Evolution of the Altaid
573 Tectonic Collage and Paleozoic Crustal Growth in Eurasia. *Nature*, 364(6435):
574 299–307
575 Shao, J. A., Tang, K. D., 1995. Terranes in Northeast China and Evolution of
576 Northeast Asia Continental Margin. Seismology Publishing House, Beijing. 185
577 (in Chinese)
578 Shcheka, S. A., Ishiwatari, A., Vrzhosek, A. A., 2001. Geology and Petrology of

579 Cambrian Khanka Ophiolite in Primorye (Far East Russia) with Notes on Its
580 Manganese-rich Chromian Spinel. *Earth Science* (Chikyu Kagaku), 55(5):
581 265–274
582 Sorokin, A. A., Kotov, A. B., Sal'nikova, E. B., et al., 2010. Granitoids of the
583 Tyrma–Bureya Complex in the Northern Bureya-Jiamusi Superterrane of the
584 Central Asian Fold Belt: Age and Geodynamic Setting. *Russian Geology and*
585 *Geophysics*, 51(5): 563–571
586 Sun, C. Y., Tang, J., Xu, W. L., et al., 2017. Crustal Accretion and Reworking
587 Processes of Micro-continental Massifs within Orogenic Belt: A Case Study of
588 the Erguna Massif, NE China. *Science China Earth Sciences*, 60(7): 1256–1267
589 Sun, D. Y., Gou, J., Wang, T. H., et al., 2013. Geochronological and Geochemical
590 Constraints on the Erguna Massif Basement, NE China-subduction History of the
591 Mongol-Okhotsk Oceanic Crust. *International Geology Review*, 55(14):
592 1801–1816
593 Sun, J. G., Chen, L., Zhao, J. K., et al., 2008. SHRIMP U–Pb Dating of Zircon from
594 Late Yanshanian Granitic Complex in Xiaoxinancha Gold-rich Copper Orefield
595 of Yanbian and Its Geological Implications. *Mineral Deposits*, 27(3): 319–328
596 (in Chinese with English Abstract)
597 Sun, S. S., McDonough, W. F., 1989. Chemical and Isotopic Systematics of Ocneanic
598 Basalts: Implications for Mantle Composition and Processes. In: Saunders, A. D.,
599 Norry, M. J., eds., Magmatism in Ocean Basins. Geological Society of Special
600 Publication, London. 42: 313–345

601 Tang, J., Xu, W. L., Wang, F., et al., 2015. Geochronology, Geochemistry, and
602 Deformation History of Late Jurassic-Early Cretaceous Intrusive Rocks in the
603 Erguna Massif, NE China: Constraints on the Late Mesozoic Tectonic Evolution
604 of the Mongol-Okhotsk Orogenic Belt. *Tectonophysics*, 658: 91–110
605 Tang, J., Xu, W. L., Wang, F., et al., 2016. Early Mesozoic Southward Subduction
606 History of the Mongol–Okhotsk Oceanic Plate: Evidence from Geochronology
607 and Geochemistry of Early Mesozoic Intrusive Rocks in the Erguna Massif, NE
608 China. *Gondwana Research*, 31: 218–240
609 Taylor, S. R., Mclennan, S. M., 1985. The Continental Crust: Its Composition and
610 Evolution, An Examination of the Geochemical Record Preserved in
611 Sedimentary Rocks. Blackwell Scientific Publications, Oxford. 312
612 Tsutsumi, Y., Yokoyama, K., Kasatkin, S. A., et al., 2014. Zircon U–Pb Age of
613 Granitoids in the Maizuru Belt, Southwest Japan and the Southernmost Khanka
614 Massif, Far East Russia. *Journal of Mineralogical and Petrological Sciences*,
615 109 (2): 97–102
616 Wang, C. Y., Campbell, I. H., Allen, C. M., et al., 2009. Rate of Growth of the
617 Preserved North American Continental Crust: Evidence from Hf and O Isotopes
618 in Mississippi Detrital Zircons. *Geochimica Et Cosmochimica Acta*, 73(3):
619 712–728
620 Wang, C. Y., Campbell, I. H., Stepanov, A. S., et al., 2011. Growth Rate of the
621 Preserved Continental Crust: II. Constraints from Hf and O Isotopes in Detrital
622 Zircons from Greater Russian Rivers. *Geochimica Et Cosmochimica Acta*, 75(5):

623 1308–1345
624 Wang, F., Xu, W. L., Gao, F. H., et al., 2012b. Tectonic History of the
625 Zhangguangcailing Group in Eastern Heilongjiang Province, NE China:
626 Constraints from U-Pb Geochronology of Detrital and Magmatic Zircons.
627 *Tectonophysics*, 566–567: 105–122
628 Wang, F., Xu, W. L., Ge, W. C., et al., 2016. The Offset Distance of the
629 Dunhua–Mishan Fault: Constraints from Paleozoic-Mesozoic Magmatism within
630 the Songnen–Zhangguangcai Range, Jiamusi and Khanka Massifs. *Acta*
631 *Petrologica Sinica*, 32 (4): 1129–1140 (in Chinese with English Abstract)
632 Wang, F., Xu, W. L., Meng, E., et al., 2012a. Early Paleozoic Amalgamation of the
633 Songnen-Zhangguangcai Range and Jiamusi Massifs in the Eastern Segment of
634 the Central Asian Orogenic Belt: Geochronological and Geochemical Evidence
635 from Granitoids and Rhyolites. *Journal of Asian Earth Sciences*, 49(3): 234–248
636 Wang, F., Xu, W. L., Xu, Y. G., et al., 2015. Late Triassic Bimodal Igneous Rocks in
637 Eastern Heilongjiang Province, NE China: Implications for the Initiation of
638 Subduction of the Paleo-Pacific Plate Beneath Eurasia. *Journal of Asian Earth*
639 *Sciences*, 97: 406–423
640 Wang, Z. W., Xu, W. L., Pei, F. P., et al., 2017. Geochronology and Geochemistry of
641 Early Paleozoic Igneous Rocks from the Zhangguangcai Range, NE China:
642 Constraints on Tectonic Evolution of the Eastern Central Asian Orogenic Belt.
643 *Lithosphere*, 9(5): 803-827
644 Windley, B. F., Alexeiev, D., Xiao, W., et al., 2007. Tectonic Models for Accretion of

the Central Asian Orogenic Belt. *Journal of the Geological Society*, 164: 31–47

Windley, B. F., Allen, M. B., Zhang, C., et al., 1990. Paleozoic Accretion and Cenozoic Redeformation of the Chinese Tien Shan Range, Central Asia. *Geology*, 18(2): 128–131

Wu, F. Y., Jahn, B. M., Wilde, S. A., et al., 2003. Highly Fractionated I-type Granites in NE China (II): Isotopic Geochemistry and Implications for Crustal Growth in the Phanerozoic. *Lithos*, 67(3–4): 191–204

Wu, F. Y., Sun, D. Y., Ge, W. C., et al., 2011. Geochronology of the Phanerozoic Granitoids in Northeastern China. *Journal of Asian Earth Sciences*, 41(1): 1–30

Wu, F. Y., Sun, D. Y., Li, H. M., et al., 2002. A-type Granites in Northeastern China: Age and Geochemical Constraints on Their Petrogenesis. *Chemical Geology*, 187(1–2): 143–173

Wu, F. Y., Sun, D. Y., Lin, Q., 1999. Petrogenesis of the Phanerozoic Granites and Crustal Growth in Northeast China. *Acta Petrologica Sinica*, 15(2):181–189 (in Chinese with English Abstract)

Wu, F. Y., Zhao, G. C., Sun, D. Y., et al., 2007. The Hulan Group: Its Role in the Evolution of the Central Asian Orogenic Belt of NE China. *Journal of Asian Earth Sciences*, 30(3): 542–556

Xiao, W. J., Windley, B. F., Hao, J., et al., 2003. Accretion Leading to Collision and the Permian Solonker Suture, Inner Mongolia, China: Termination of the Central Asian Orogenic Belt. *Tectonics*, 22(6): 8-1–8-6

Xiao, W. J., Zhang, L. C., Qin, K. Z., et al., 2004. Paleozoic Accretionary and

667 Collisional Tectonics of the Eastern Tianshan (China): Implications for the
668 Continental Growth of Central Asia. *American Journal of Science*, 304: 370–395
669 Xu, M. J., Xu, W. L., Wang, F., et al., 2013. Geochronology and Geochemistry of the
670 Early Jurassic Granitoids in the Central Lesser Xing'an Range, NE China and Its
671 Tectonic Implications. *Acta Petrologica Sinica*, 29: 354–368 (in Chinese with
672 English Abstract)
673 Xu, T., Xu, W. L., Wang, F., et al., 2017. Geochronology and Geochemistry of Early
674 Paleozoic Intrusive Rocks from the Khanka Massif of the Russian Far East:
675 Petrogenesis and Tectonic Implications. *Lithos*, in press
676 Xu, W. L., Ji, W. Q., Pei, F. P., et al., 2009. Triassic Volcanism in Eastern Heilongjiang
677 and Jilin Provinces, NE China: Chronology, Geochemistry, and Tectonic
678 Implications. *Journal of Asian Earth Sciences*, 34(3): 392–402
679 Xu, W. L., Pei, F. P., Wang, F., et al., 2013. Spatial-temporal Relationships of
680 Mesozoic Volcanic Rocks in NE China: Constraints on Tectonic Overprinting
681 and Transformations between Multiple Tectonic Systems. *Journal of Asian Earth*
682 *Sciences*, 74(18): 167–193
683 Yakubchuk, A., 2004. Architecture and Mineral Deposit Settings of the Altaid
684 Orogenic Collage: A Revised Model. *Journal of Asian Earth Sciences*, 23(5):
685 761–779
686 Yang, H., Ge, W. C., Zhao, G. C., et al., 2015b. Late Triassic Intrusive Complex in the
687 Jidong Region, Jiamusi-Khanka Block, NE China: Geochemistry, Zircon U–Pb
688 Ages, Lu–Hf Isotopes, and Implications for Magma Mingling and Mixing. *Lithos*,

224–225: 143–159

Yang, H., Ge, W. C., Zhao, G. C., et al., 2015a. Early Permian-Late Triassic Granitic Magmatism in the Jiamusi–Khanka Massif, Eastern Segment of the Central Asian Orogenic Belt and Its Implications. *Gondwana Research*, 27(4): 1509–1533

Yang, J. H., Wu, F. Y., Shao, J. A., et al., 2006. Constraints on the Timing of Uplift of the Yanshan Fold and Thrust Belt, North China. *Earth and Planetary Science Letters*, 246(3): 336–352

Yarmolyuk, V. V., Kovalenko, V. I., Salnikova, E. B.,et al., 2002. Tectono-magmatic Zoning, Magma Sources, and Geodynamics of the Early Mesozoic Mongolia-Transbaikal Province. *Geotectonics*, 36(4): 293–311

Yu, J. J., Wang, F., Xu, W. L., et al., 2012. Early Jurassic Mafic Magmatism in the Lesser Xing'an-Zhangguangcai Range, NE China and Its Tectonic Implications: Constrains from Zircon U-Pb Chronology and Geochemistry. *Lithos*, 142–143: 256–266

Zhao, Y. D., Chi, X. G., Che, J. Y., et al., 2009. Geochemical Characteristics and Tectonic Setting of the Late Triassic Granites in Yanbian-Dongning Area. *Journal of Jilin University*, 39(3): 425–434 (in Chinese with English abstract)

Zhou, J. B., Wilde, S. A., Zhao, G. C., et al., 2010. Was the Easternmost Segment of the Central Asian Orogenic Belt Derived from Gondwana or Siberia: An Intriguing Dilemma? *Journal of Geodynamics*, 50: 300–317